

MOLECULAR DYNAMICS MODELING OF STRUCTURAL BATTERY COMPONENTS

Osvalds Verners¹, Adri C. T. van Duin², Marnix Wagemaker³, Angelo Simone⁴

¹ Department of Structural Engineering, Faculty of Civil Engineering and Geosciences
Delft University of Technology
Stevinweg 1, 2628 CN Delft, The Netherlands
Email: o.verners@tudelft.nl

² Department of Mechanical and Nuclear Engineering, Pennsylvania State University
136 Research East Building, University Park PA 16802, USA
Email: acv13@psu.edu, web page: www.engr.psu.edu/adri

³ Department of Radiation Science and Technology, Faculty of Applied Sciences
Delft University of Technology
Mekelweg 15, 2629 JB Delft, The Netherlands
Email: m.wagemaker@tudelft.nl

⁴ Department of Structural Engineering, Faculty of Civil Engineering and Geosciences
Delft University of Technology
Stevinweg 1, 2628 CN Delft, The Netherlands
Email: a.simone@tudelft.nl, web page: <http://cm.strumech.citg.tudelft.nl/simone>

Keywords: Solid polymer electrolyte, Molecular dynamics, Li ion diffusivity, Plasticizer

ABSTRACT

A crosslinked polymer based solid electrolyte prototype material –poly(propylene glycol) diacrylate– is studied using the reactive molecular dynamics force field ReaxFF. The focus of the study is the evaluation of the effects of equilibration and added plasticizer (ethylene carbonate) or anion (PF_6^-) components on Li ion transport properties in the solid electrolyte. The study includes initial evaluation of the force field, including bond dissociation characteristics, relevant for material failure, and elastic properties at room temperature, relevant for the structural application purpose.

All considered systems indicate enhancement of Li ion diffusivity with respect to the 1 atm equilibrated system without additives/anions. Based on Li-O radial distribution function and integral radial distribution function comparisons, this is attributed to differences in Li solvation structure and related plastification, complexation and solvent exchange mechanisms.

1 INTRODUCTION

Following recent [1–5] technological developments, structural batteries have attracted attention as a potential multifunctional composite material [6]. As a further development, a three-dimensional battery architecture for structural applications, based on earlier generic concepts [7, 8], has been proposed [3]. The architecture consists in the integration of both electrode materials into an interpenetrating monolith structure using a thin solid electrolyte layer as the separator. The latter element offers a distinct advantage over conventional laminate structural battery prototypes due to significant reduction of ionic transport distance in the solid electrolyte, which is known to have low ionic conductivity, as compared to liquid electrolytes in conventional Li ion batteries [4]. Accordingly, a need has arisen for computationally analyzing and improving the properties of potential battery component materials and composite

structures made thereof. As a result, a number of studies have focused on polymer electrolytes [9–18], considering Li ion transport mechanisms and effects of plasticizers among others. In this paper, the results of a molecular dynamics (MD) analysis of a prototype solid electrolyte derived material [19] –poly(propylene glycol) diacrylate (PPGDA)– will be presented. This study aims to gain an atomistic level insight of the macroscopic mechanical and electrical properties of the material and the correlations between them.

2 METHOD

2.1 Structures

Crosslinked and noncrosslinked PPGDA polymer structures (Figure 1a) were created using Molden [20], Packmol [21] and LAMMPS [22, 23]. An orthogonal unit cell of 520 atoms with minimum average dimensions of 17.2 Å and 17.7 Å (at 1 atm), respectively, was used. Lithium atoms at a ratio of $\text{Li}:(\text{PO} + \text{A}) = 1:18.7$ (PO = propylene oxide groups, A = acrylate groups) were added during a constant volume MD simulation at a frequency of 0.004 fs^{-1} after equilibration at constant pressure (1 atm). The unit cell was expanded $2 \times 2 \times 2$ times (size effects considered in Section 3.2). The structures consisted of a mixture of periodic poly(propylene glycol) (PPG) and single PPG unit PPGDA monomers. For crosslinking, the carbon atoms of the methyl group branches of PPG were bonded with the terminal double-bonded carbon atoms of the PPGDA oligomer acrylate groups. The latter crosslink formation energy had been found to be lower than that of an alternative, backbone carbon bonded, crosslinking (Table 1). Thereby, a periodic crosslinking level of 50% with respect to the total number of double bonds in the system was obtained (Figure 1b).

For the evaluation of plasticizer and supporting electrolyte effects on Li ion diffusivity, crosslinked systems with ethylene carbonate (EC) molecules, ratio $\text{Li}:\text{EC}=1:4$ (corresponding to 24 wt %), and LiPF_6 salt anions, ratio $\text{Li}:\text{P}=1:1$, respectively, were studied along with a lithiated structure without additives or anions.

2.2 Simulation settings

MD simulations were performed with LAMMPS [22, 23]. The empirical reactive force field ReaxFF [24] with a parameter set for the elements C, O, H, F, Li, S [25] was used. By employing this force field, LiPF_6 diffusivities in EC solvent in good agreement with density functional theory (DFT) MD

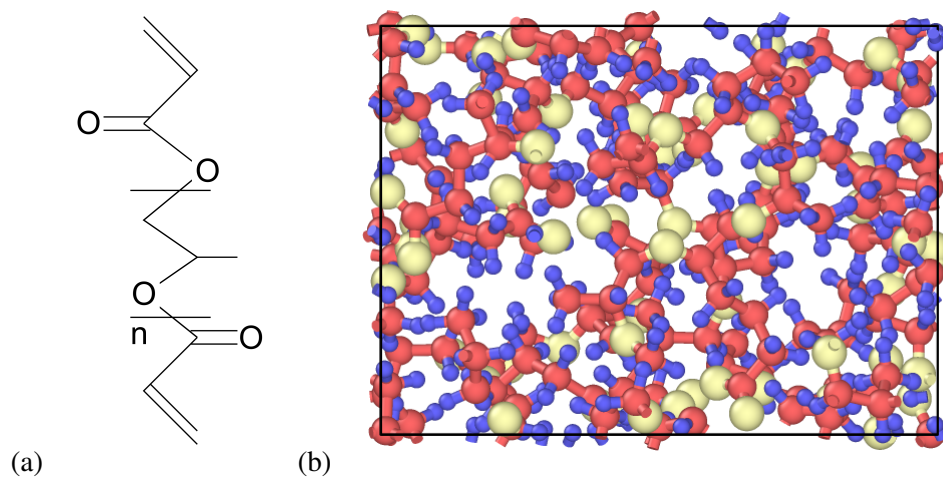


Figure 1: PPGDA oligomer structure (a) and crosslinked PPGDA polymer 520-atom unit cell (C=red, H=blue, O=yellow) (b).

results [26] have been obtained.

The structures were initially energy minimized using a conjugate gradient method (max. force convergence criterion of $1\text{e-}6$ kcal/mol/Å) combined with quadratic linesearch (max. displacement of $1\text{e-}2$ Å per outer iteration) [27]. Minimization was stopped if linesearch $\alpha = 0$ was reached. For finite temperature equilibration at 300K and 1 atm, the Nose-Hoover thermo/barostat was coupled with five chain thermostats [27, 28] (LAMMPS equivalent temperature damping constant of 100 fs and pressure damping constants of 250 fs and 25 fs for crosslinked and noncrosslinked structures, respectively, were used) to simulate the isothermal/isobaric (NPT) ensemble. Anisotropic pressure equilibration was applied. For the subsequent diffusivity calculation simulations, the Nose-Hoover thermostat was applied to simulate the canonical (NVT) ensemble. All MD simulations were performed using Verlet type time integration [29] with a 0.25 fs time step.

For validation against DFT results, ionic relaxation calculations were performed using the VASP simulation package [30,31]. For the calculations, the plane augmented wave (PAW) [32,33] implementation was used with the generalized gradient approximation (GGA) PBE exchange-correlation functional [34], DFT D3 van der Waals interaction correction method with Becke-Jonson damping [35] (for condensed phase structures), $1\text{e-}4$ eV convergence criterion for combined Davidson block iteration [36] / residual minimization method direct inversion in the iterative subspace [37] electronic minimization, and a conjugate gradient energy convergence criterion of $1\text{e-}4$ eV for the ionic relaxation [38]. For band-structure energy calculations, the linear tetrahedron method with Bloechel corrections [39] and Gauss-like functions [40] with the parameter $\sigma = 0.05$ [38] were used for multiple and less-than-five k -point grids, respectively. For k -point grid definitions, the Monkhorst-Pack scheme [41] was used. 400/520 eV plane wave basis set cutoffs were used for constant/variable cell volume calculations, respectively.

2.3 Analysis methods

The Li ion and P atom self-diffusivities, where P atoms represent PF_6^- ions, were calculated according to the Einstein relation [42] using a least squares curve fit approach after constant volume equilibration. A sliding window algorithm using 1000 sample trajectories from 25 fs simulations was adapted from [42].

The Young's modulus of PPGDA at 0K was estimated according to the Reuss and Voigt theories [43], based on compliance and elasticity constant values, respectively. The solvation characteristics of the obtained structures were compared by calculating the Li-O and Li-P radial distribution functions (RDF) $g(r)$ and radial integrals of RDFs (IRDF) $\text{Int}(g(r))$, using a sampling bin size of 0.1 Å, averaged over 14 ps from 25 ps trajectories.

3 RESULTS AND DISCUSSION

3.1 Force field validation

The ReaxFF force field was evaluated by comparing the reaction energy for the assumed crosslinking reaction energies (Table 1) and dissociation path energies of PPGDA monomers and PPG polymers against DFT calculations (Figure 2). Macroscopic physical properties, including density and Young's modulus at room temperature were compared against experimental values (Table 2). Distinct differences in dissociation barrier and reaction energies suggest that a weaker overall material response beyond elasticity range (inelastic material response) could be predicted than expected according to the DFT results. In contrast, a reasonable agreement was found for the oligomer weight extrapolation based Young's modulus estimate. This was supported by the observed agreement with DFT dissociation energy curves within the elastic response range (Figure 3a). Overestimation of material density, especially for noncrosslinked polymer, was partially attributed to stronger nonbonded interaction predictions (Figure 3b).

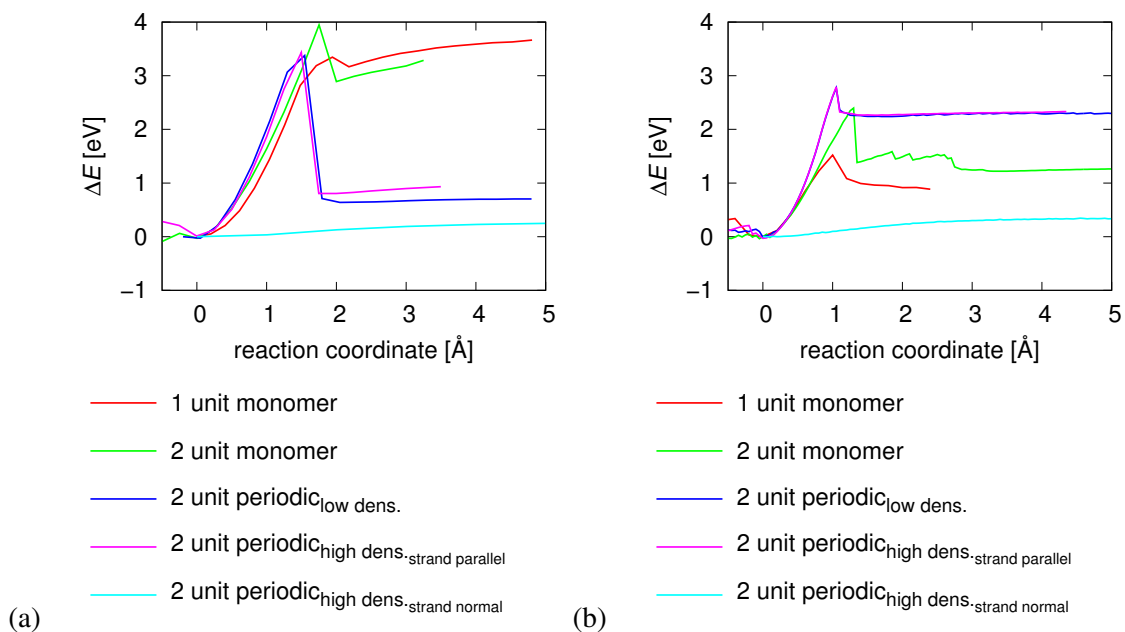


Figure 2: Comparison of DFT (a) and ReaxFF (b) PPGDA/PPG monomer/polymer dissociation path energies.

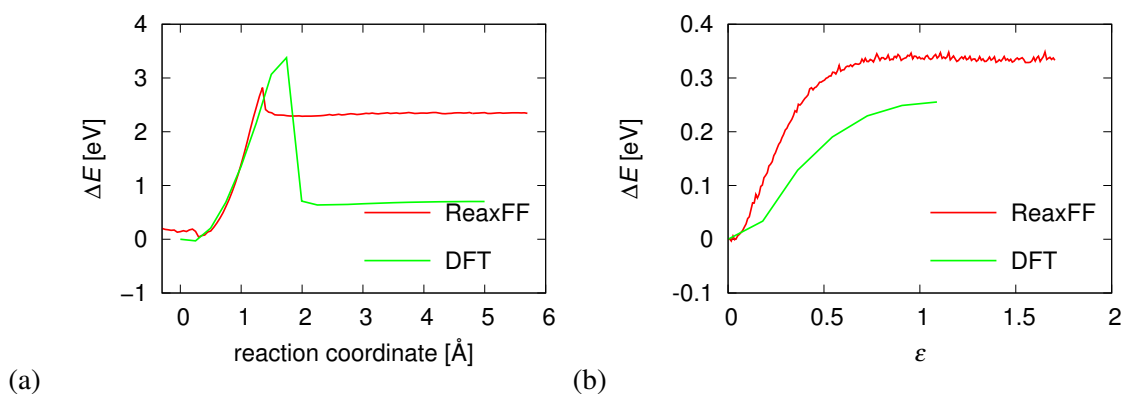


Figure 3: Comparison of DFT and ReaxFF dissociation path energies for two PPG units at dilute limit density in strand direction (a) and at condensed phase density in strand normal direction (b).

| structure | ReaxFF | DFT |
|--------------------|--------|------------------------|
| branch crosslink | 0.63 | 0.98 |
| backbone crosslink | 0.22 | 0.95/0.72 ^a |

^a local minimum

Table 1: PPGDA crosslinking energies [eV].

| | ReaxFF | experiment |
|--|------------------------|--|
| mass density [g/cm^3] ^e | 1.13-1.15 ^a | 1.01-1.03 ^b [44] 1.065 ^c [45] |
| glass transition temperature [$^{\circ}\text{C}$] | -13 | -43 [46] |
| Young's modulus [MPa] ^e | 90 | 99 ^d [47] |

^a crosslinked/noncrosslinked

^b noncrosslinked

^c crosslinked

^d exponential extrapolation of oligomer molecular weight

^e room temperature

Table 2: PPGDA physical properties.

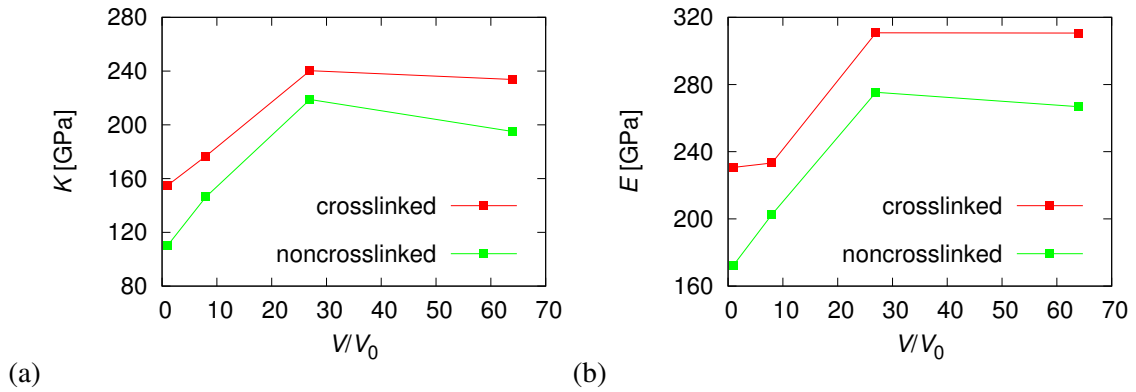


Figure 4: PPGDA bulk modulus (K) (a) and Young's modulus (E) (b) vs volume expansion ($V_0 = 4912 \text{ \AA}^3$) at 0K.

3.2 Size and strain rate effects

Size effects were estimated by comparing the elastic material response at three expansion levels with respect to the unit cell at 0K and at room temperature (300K). The 0K Young's modulus estimate, calculated as the mean of moduli that corresponded to 1e3 and 1e4 strain increments, indicates that size convergence is reached at around two-three expansion levels (Figure 4). Size effects at room temperature were evaluated only for the crosslinked system since the noncrosslinked system possessed no observable elastic strength at the considered loading rates. Referring to the distribution of line fit residuals of the Young's modulus calculation for the crosslinked systems (Figure 5), it was observed that larger systems tend to yield higher minimum stiffness and reduced residuals, hence the largest minimum stiffness was considered as the most accurate. Based on these, convergence was assumed to occur at three-four expansion levels. For further study, the $2 \times 2 \times 2$ expanded crosslinked system was used.

Strain rate effects were evaluated for the $2 \times 2 \times 2$ expanded system by applying tensile deformation rates of 30/3/0.3 $\text{\AA}/\text{fs}$ with respect to the system's dimension parallel to the deformation direction – these values correspond to the range of rates that were computationally feasible. The results indicate no significant dependence on strain rates (Figure 6), which is considered as sufficient for validating the obtained Young's modulus comparison with experimental data (Table 2). The latter result is also in agreement with predictions of dynamic moduli according to experimental results from dynamic bending loading at high loading frequency limit [45].

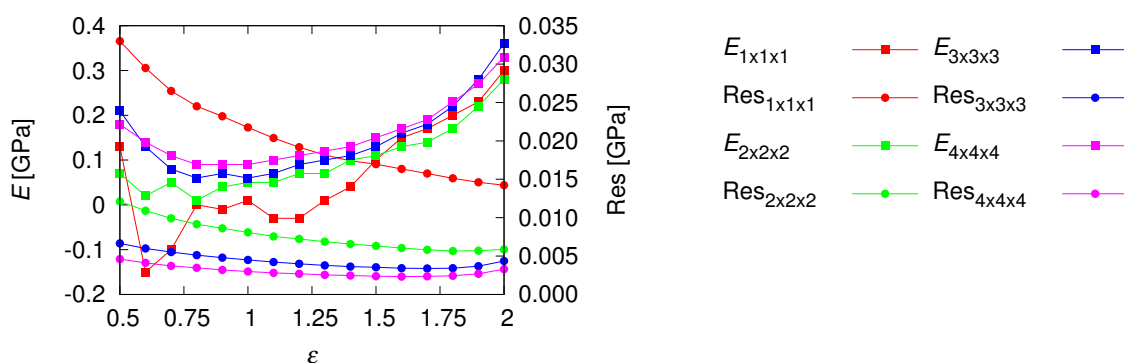


Figure 5: PPGDA Young's modulus (E) and normalized line fit residual (Res) vs calculation reference strain (engineering strain ϵ) for different unit cell expansions ($V_0 = 4912 \text{ \AA}^3$) at 300K.

3.3 Equilibration effects

The equilibration effects were estimated by comparing the crosslinked lithiated structures with and without NPT equilibration after lithiation. The latter structure was uniformly scaled to the 1 atm equivalent density (1.11 g/cm^3); in application terms, this would approximate the system state during rapid lithiation or high strain rate deformation. An order of magnitude difference in Li ion diffusivities was observed (Table 3). Furthermore, it was observed that the first two coordination shells (designated by the IRDF plateaus at 2.5 \AA and 3.3 \AA) for both structures are loosely similar (Figure 7). However, significantly less transition states were observed for the NPT equilibrated structure, due to the close-to-zero RDF value at approximately 3.3 \AA , which is seen as indicative of more stable local solvation structure. This is assumed to inhibit Li ion diffusion by migration along polymers and by solvent exchange, the latter being considered significant for Li ion mobility in similar polymers without plasticizers [9, 10]. The structural differences may also explain the difference in potential energies of both structures, that of the NPT equilibrated structure being approximately 3% lower.

3.4 Plasticizer and anion effects

The results in Table 3 indicate that for the system with EC plasticizer the Li ion diffusivity value was significantly higher than for the same system without plasticizer. The difference is attributed to the formation of higher coordinated first coordination shell (designated by the IRDF plateau at 2.5 \AA) with

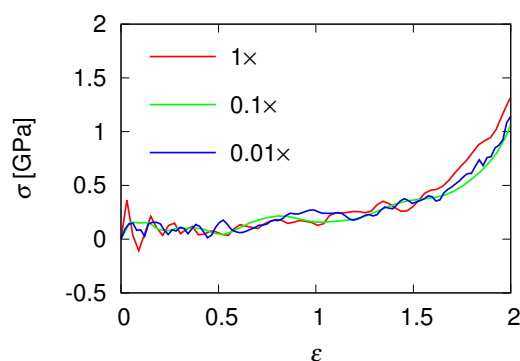


Figure 6: Bezier interpolated PPGDA tensile stress (σ) vs engineering strain (ϵ) for different strain rates ($1 \times = 30 \text{ \AA/fs}$).

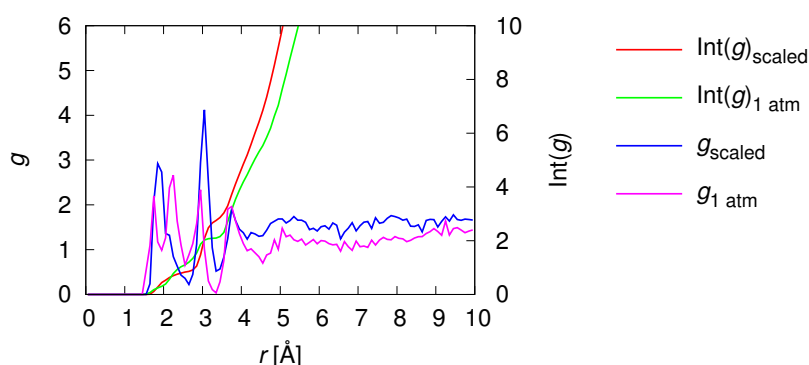


Figure 7: Li-O RDFs and IRDFs for Li/PPGDA at 1.11 g/cm³ (1 atm –NPT equilibrated system, scaled –NVT equilibrated scaled system).

| solvent/additive/anion | ρ [g/cm ³] | D [cm ² /s] |
|--------------------------------------|-----------------------------|---|
| PPGDA/-/- | 1.11 | 6.89e-07 ^a / 5.30e-06 ^b |
| PPGDA/-/PF ₆ ⁻ | 1.16 | 7.95e-07 |
| PPGDA/EC/- | 1.16 | 3.37e-06 |

^a 1 atm equilibrated system

^b NVT equilibrated scaled system

Table 3: Li ion diffusivity comparison for different solvent systems.

a higher minimum Li-O distance (Figure 8). This was found to be in line with the findings that EC can form stable solvation structures for Li in pure EC [26]. The latter, in combination with the preserved low RDF value delimiting the second coordination shell at approximately 3.3 Å, suggests a reduction of the probability of ion transport through solvent exchange [12, 13]. Subsequently, it was concluded that the enhancement of diffusivity is achieved through reduced Li interaction with PPGDA O atoms and complexation with EC molecules, in analogy with TFSI⁻/EC complexation studied in a poly(ethylene oxide) (PEO) based electrolyte [14]. The latter assumption is supported by the similar value of carbonyl oxygen based estimate of EC diffusivity (2.49e-06 cm²/s).

For the system with PF₆⁻ anions, we observe that the first coordination shell (designated by the IRDF plateau at 2.5 Å) indicates a lower coordination than for the system without anions (Figure 9). Moreover, both bonded and non-bonded Li-P coordinations are observed, which suggests that the observed small increase in Li ion diffusivity (Table 3) is linked to interactions with PF₆⁻ ions and subsequent Li-O coordination weakening, the low RDF value at 3.3 Å, which delimits the second coordination shell, being preserved. Furthermore, both Li-P RDF based equilibrium distances were found to be similar to the DFT MD results for LiPF₆/EC liquid solutions [26]. Since the PF₆⁻ diffusivity (2.93e-07 cm²/s) was found to be lower than that of Li (Table 3), the main Li ion transport mechanism was linked to PF₆⁻ facilitated solvent exchange.

4 CONCLUSIONS

The force field evaluation indicates good agreement with reference data for elastic properties of PPGDA both at dilute limit and condensed phase densities. The differences that were found for bond energies and dissociation barriers indicate potential improvement areas for the force field applications in inelastic deformation simulations.

The study has provided insights into the role of equilibration and plasticizer or anion components on Li ion transport properties in a solid electrolyte prototype material. As expected, the system with

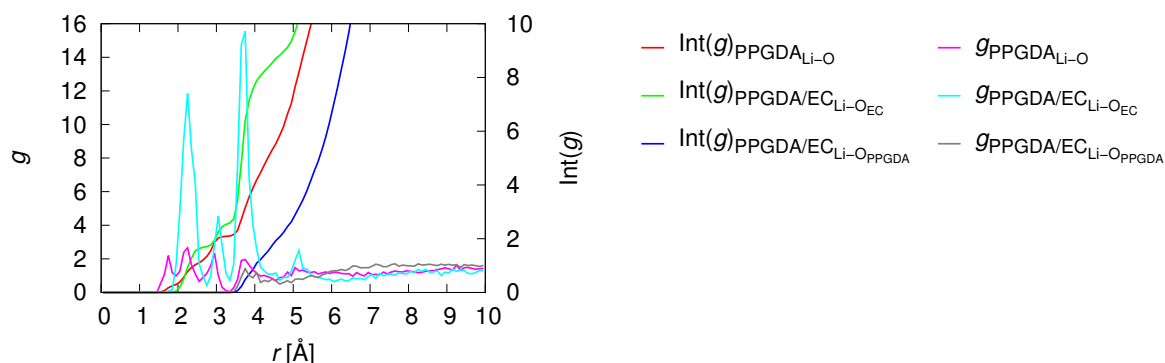
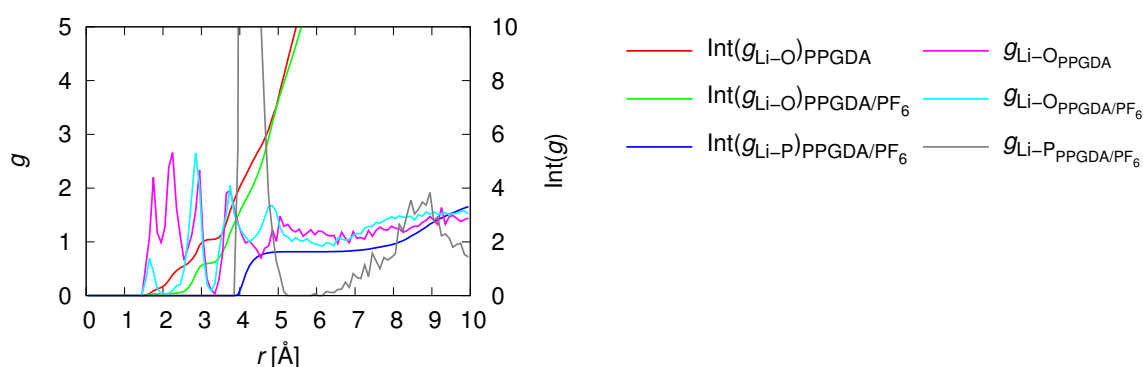


Figure 8: Li-O RDFs and IRDFs for Li/PPGDA and Li/PPGDA/EC (densities correspond to 1 atm).


 Figure 9: Li-O RDFs and IRDFs for Li/PPGDA and PPGDA/LiPF₆ (densities correspond to 1 atm).

plasticizer additive, as well as the system under dynamic loading conditions, indicates a significant enhancement of Li ion diffusivity, whereas the system with anions indicates no significant change Li ion diffusivity. The latter conclusions were made considering the expected $\sim 50\%$ uncertainty in predicted ion diffusivity values due to the simulation timescales of organic liquid electrolyte systems [26].

Based on Li-O RDF and IRDF comparison, the distinctions in diffusivity are attributed to differences in Li solvation structure, complexation and additive facilitated or inhibited Li ion transport mechanisms, including solvent exchange and diffusion along polymer chains.

ACKNOWLEDGEMENTS

The research leading to these results has received funding from the European Research Council under the European Union's Seventh Framework Programme (FP7/2007-2013) / ERC Grant agreement n° 617972.

REFERENCES

- [1] F. Gasco and P. Feraboli. Manufacturability of composite laminates with integrated thin film Li-ion batteries. *Journal of Composite Materials*, 48(8):899–910, 2014.
- [2] M. Willgert, M. H. Kjell, E. Jacques, M. Behm, G. Lindbergh, and M. Johansson. Photoinduced free radical polymerization of thermoset lithium battery electrolytes. *European Polymer Journal*, 47(12):2372–2378, 2011.
- [3] S. Leijonmarck, T. Carlson, G. Lindbergh, L. E. Asp, H. Maples, and A. Bismarck. Solid polymer

- electrolyte-coated carbon fibres for structural and novel micro batteries. *Composites Science and Technology*, 89:149–157, 2013.
- [4] L. E. Asp and E. S. Greenhalgh. Structural power composites. *Composites Science and Technology*, 101:41–61, 2014.
- [5] E. L. Wong, D. M. Baechle, K. Xu, R. H. Carter, J. F. Snyder, and E. D. Wetzel. Design and processing of structural composite batteries. *International SAMPE Symposium and Exhibition (Proceedings)*, 52, 2007.
- [6] Volvo Car Group. Nano battery project, 2015.
- [7] N.S. Ergang, M.A. Fierke, Z. Wang, W.H. Smyrl, and A. Stein. Fabrication of a fully infiltrated three-dimensional solid-state interpenetrating electrochemical cell. *Journal of the Electrochemical Society*, 154(12):A1135–A1139, 2007.
- [8] B. Dunn, J.W. Long, and D.R. Rolison. Rethinking multifunction in three dimensions for miniaturizing electrical energy storage. *Electrochemical Society Interface*, 17(3):49–53, 2008.
- [9] D. Diddens, A. Heuer, and O. Borodin. Understanding the lithium transport within a Rouse-based model for a PEO/LiTFSI polymer electrolyte. *Macromolecules*, 43(4):2028–2036, 2010.
- [10] A. Maitra and A. Heuer. Cation transport in polymer electrolytes: A microscopic approach. *Physical Review Letters*, 98(22), 2007.
- [11] D. Diddens and A. Heuer. Lithium ion transport mechanism in ternary polymer electrolyte-ionic liquid mixtures: A molecular dynamics simulation study. *ACS Macro Letters*, 2(4):322–326, 2013.
- [12] O. Borodin and G.D. Smith. Li⁺ transport mechanism in oligo(ethylene oxide)s compared to carbonates. *Journal of Solution Chemistry*, 36(6):803–813, 2007.
- [13] D. Diddens and A. Heuer. Simulation study of the lithium ion transport mechanism in ternary polymer electrolytes: The critical role of the segmental mobility. *Journal of Physical Chemistry B*, 118(4):1113–1125, 2014.
- [14] H. Wu and C.D. Wick. Computational investigation on the role of plasticizers on ion conductivity in poly(ethylene oxide) LiTFSI electrolytes. *Macromolecules*, 43(7):3502–3510, 2010.
- [15] H. Wu, O.T. Cummings, and C.D. Wick. Computational investigation on the effect of alumina hydration on lithium ion mobility in poly(ethylene oxide) LiClO₄ electrolytes. *Journal of Physical Chemistry B*, 116(51):14922–14932, 2012.
- [16] D. Brandell, H. Kasemgi, T. Tamm, and A. Aabloo. Molecular dynamics modeling the Li-PolystyreneTFSI/PEO blend. *Solid State Ionics*, 262:769–773, 2014.
- [17] L.J.A. Siqueira and M.C.C. Ribeiro. Molecular dynamics simulation of the polymer electrolyte poly(ethylene oxide) LiClO₄. I. structural properties. *Journal of Chemical Physics*, 122(19), 2005.
- [18] O. Borodin and G.D. Smith. Molecular dynamics simulations of comb-branched poly(epoxide ether)-based polymer electrolytes. *Macromolecules*, 40(4):1252–1258, 2007.
- [19] B. Sun, D. Rehnlund, M.J. Lacey, and D. Brandell. Electrodeposition of thin poly(propylene glycol) acrylate electrolytes on 3D-nanopillar electrodes. *Electrochimica Acta*, 137(0):320–327, 2014.
- [20] G. Schaftenaar and J.H. Noordik. Molden: a pre- and post-processing program for molecular and electronic structures. *Journal of Computer-Aided Molecular Design*, 14(2):123–134, 2000.

- [21] L. Martnez, R. Andrade, E. G. Birgin, and J. M. Martnez. PACKMOL: A package for building initial configurations for molecular dynamics simulations. *Journal of Computational Chemistry*, 30(13):2157–2164, 2009.
- [22] S. Plimpton. Fast parallel algorithms for short-range molecular dynamics. *Journal of Computational Physics*, 117(1):1–19, 1995.
- [23] H. M. Aktulga, J. C. Fogarty, S. A. Pandit, and A. Y. Grama. Parallel reactive molecular dynamics: Numerical methods and algorithmic techniques. *Parallel Computing*, 38(4-5):245–259, 2012.
- [24] A. C. T. van Duin, S. Dasgupta, F. Lorant, and W. A. Goddard. ReaxFF: a reactive force field for hydrocarbons. *The Journal of Physical Chemistry A*, 105(41):9396–9409, 2001.
- [25] M.M. Islam, V.S. Bryantsev, and A.C.T. van Duin. ReaxFF reactive force field simulations on the influence of teflon on electrolyte decomposition during Li/SWCNT anode discharge in lithium-sulfur batteries. *Journal of the Electrochemical Society*, 161(8):E3009–E3014, 2014.
- [26] M. T. Ong, O. Verners, E. W. Draeger, A. C. T. van Duin, V. Lordi, and J. E. Pask. Lithium ion solvation and diffusion in bulk organic electrolytes from first-principles and classical reactive molecular dynamics. *The Journal of Physical Chemistry B*, 119(4):1535–1545, 2015. PMID: 25523643.
- [27] Sandia National Laboratories. LAMMPS documentation, 2015.
- [28] W. Shinoda, M. Shiga, and M. Mikami. Rapid estimation of elastic constants by molecular dynamics simulation under constant stress. *Physical Review B*, 69:134103, 2004.
- [29] M.E. Tuckerman, J. Alejandre, R. Lopez-Rendn, A. L. Jochim, and G. J. Martyna. A liouville-operator derived measure-preserving integrator for molecular dynamics simulations in the isothermal-isobaric ensemble. *Journal of Physics A: Mathematical and General*, 39(19):5629, 2006.
- [30] G. Kresse and J. Hafner. *Ab initio* molecular dynamics for liquid metals. *Physical Review B*, 47:558–561, 1993.
- [31] G. Kresse and J. Furthmüller. Efficient iterative schemes for *ab initio* total-energy calculations using a plane-wave basis set. *Physical Review B*, 54:11169–11186, 1996.
- [32] P. E. Blöchl. Projector augmented-wave method. *Physical Review B*, 50:17953–17979, 1994.
- [33] G. Kresse and D. Joubert. From ultrasoft pseudopotentials to the projector augmented-wave method. *Physical Review B*, 59:1758–1775, 1999.
- [34] J. P. Perdew, K. Burke, and M. Ernzerhof. Generalized gradient approximation made simple. *Physical Review Letters*, 77:3865–3868, Oct 1996.
- [35] S. Grimme, S. Ehrlich, and L. Goerigk. Effect of the damping function in dispersion corrected density functional theory. *Journal of Computational Chemistry*, 32(7):1456–1465, 2011.
- [36] S. Wilson and G. H. F. Diercksen. *Methods in Computational Molecular Physics*. Nato Science Series B. Springer, 2013.
- [37] P. Pulay. Convergence acceleration of iterative sequences. The case of SCF iteration. *Chemical Physics Letters*, 73(2):393–398, 1980.
- [38] G. Kresse, M. Marsman, and J. Furthmüller. VASP documentation, 2015.

- [39] P. E. Blöchl, O. Jepsen, and O. K. Andersen. Improved tetrahedron method for Brillouin-zone integrations. *Phys. Rev. B*, 49:16223–16233, 1994.
- [40] A. De Vita and M. J. Gillan. The energetics of hydrogen in aluminium calculated from first principles. *Journal of Physics: Condensed Matter*, 4(2):599, 1992.
- [41] H. J. Monkhorst and J. D. Pack. Special points for Brillouin-zone integrations. *Physical Review B*, 13:5188–5192, 1976.
- [42] D. Frenkel and B. Smit. *Understanding molecular simulation: From algorithms to applications*. Academic Press, 1996.
- [43] R. Hill. The elastic behaviour of a crystalline aggregate. *Proceedings of the Physical Society. Section A*, 65(5):349–354, 1952.
- [44] Sigma-Aldrich Co. LLC. Online catalog, 2015.
- [45] R. D. Raharjo, H. Lin, D. F. Sanders, B. D. Freeman, S. Kalakkunnath, and D. S. Kalika. Relation between network structure and gas transport in crosslinked poly(propylene glycol diacrylate). *Journal of Membrane Science*, 283(12):253–265, 2006.
- [46] S. Kalakkunnath, D. S. Kalika, H. Lin, R. D. Raharjo, and B. D. Freeman. Molecular dynamics of poly(ethylene glycol) and poly(propylene glycol) copolymer networks by broadband dielectric spectroscopy. *Macromolecules*, 40(8):2773–2781, 2007.
- [47] N. P. Patel, C. M. Aberg, A. M. Sanchez, M. D. Capracotta, J. D. Martin, and R. J. Spontak. Morphological, mechanical and gas-transport characteristics of crosslinked poly(propylene glycol): homopolymers, nanocomposites and blends. *Polymer*, 45(17):5941–5950, 2004.